Int J Adv Manuf Technol (2017) 90:45–57
DOI 10.1007/s00170-016-9279-8

ORIGINAL ARTICLE

Sensitivity analysis on ram speed of a direct extrusion process model using a porthole die through CEL method

M. Cristobal[1] · E. I. Ramírez[1] · O. Ruiz[1] · A. Ortiz[1] · V. H. Jacobo[1]

Received: 10 April 2016 / Accepted: 1 August 2016 / Published online: 26 August 2016

Abstract In this paper, a tube extrusion process by finite element was analyzed, using coupled Eulerian-Lagrangian method (CEL) due to the severe deformation that material presents and thereby avoids distortion of the mesh and adaptive meshing used in Lagrangian models, in order to obtain stress distribution, strains, extrusion force, and flow material behavior. Four isothermal models were performed by modifying the sensitivity of ram speed using discrete rigid tools with general contact option to simulate the interaction between them; 7005 aluminum was considered as the material to be extruded. In order to reduce high computational time application, speed was increased to observe its influence on the results, in other words the variations between the models. As a consequence of this analysis, it was found that while the kinetic energy does not exceed 5 to 10 % of whole internal energy, material flow behavior and stress level are not affected.

Keywords FEM analysis · Coupled Eulerian-Lagrangian (CEL) · Pipe extrusion · Porthole die

✉ M. Cristobal
fi.cristobal@live.com

E. I. Ramírez
isaac10@unam.mx

O. Ruiz
oruiz@unam.mx

A. Ortiz
armandoo@unam.mx

V. H. Jacobo
vjacobo@dgapa.unam.mx

[1] Unidad de Investigación y Asistencia Técnica en Materiales, Facultad de Ingeniería, UNAM, Laboratorios de Ingeniería Mecánica "Ing. Alberto Camacho Sánchez", Circuito interior, Anexo de Ingeniería, Ciudad Universitaria, Mexico 04510, D.F., Mexico

1 Introduction

During the past 37 years, mathematical models and aluminum extrusion simulations have been reported [1], although the industry is over a hundred years old. Most researches focus on 2D or 3D simple geometries considering symmetries, due to the need of high-level computational capacity.

To produce seamless tubes with small tolerances by extrusion process, a mandrel in the stem end is used, which forces material to flow through, forming the internal tube geometry. This technique is applied in 6xxx and 7xxx series aluminum alloys owing to exhibit low shear stress at extrusion temperature; however, the arduousness of correctly centering mandrel causes the non-homogeneous thickness [2].

Another way to produce seamless tubes is by tool stack, in which a small length element within it serves as a mandrel; the upper die generates a distributed feeds series, so the contact with each other are welded by temperature and pressure into a single flow around the mandrel (Fig. 1).

Tube thickness is adjusted according to the hollow generated between the mandrel and the lower die circular section. This process allows to get very long sections with

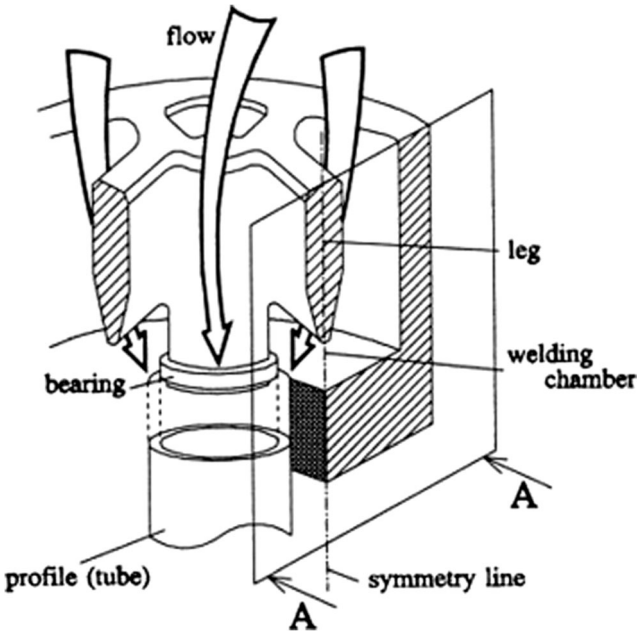

Fig. 1 Schematic tube extrusion process [3]

accuracy of shape and dimensions used in complex hollow heat exchangers.

In order to use this kind of dies to do extrusion, the experience of designers using empirical rules is quite needed, which greatly depends on personal judgment, intuition, and experience [4]. It is complex to analyze material behavior inside those dies; implementation of finite element software can reveal the distribution and evolution of plastic deformation, extrusion force, extrusion speed, and effective stress.

Kloppenborg et al. [5] proposed a viscoplastic analysis of the material flow inside a porthole die; Li et al. [6] used numerical codes to predict meaningful process variables inside the welding chamber. Due to the process complexity, some researchers have proposed simplified tests, based on flat rolling [7] or proper compressive processes [8] in order to carry out a number of experimental investigations.

Gagliardi et al. [9] investigated the role of process parameters affecting the process load and welding criteria, Junquan et al. [10] performed a quarter of the numerical simulation model with Deform 3D software, and Zhang et al. [11] proposed a mesh-reconstruction technology because of its inability to deal with meshes separation and penetration during welding.

Coupled Eulerian-Lagrangian method (CEL) is an analysis technique used in fluid dynamics and heat transfer; the use of this formulation avoids problems that other techniques present, such as distortion mesh. This feature is useful when forming processes like aluminum extrusion profiles are modeled; for this reason, it is used in this paper [12].

Abaqus 6.14 ® software was used; it has the tool called coupled Eulerian-Lagrangian method which is an easy-to-use feature of Abaqus/Explicit general contact which enables fully coupled multi-physics simulation such as fluid-structure interaction [13].

Lagrangian and Eulerian elements can be combined in the same model using a technique known as CEL analysis. In a CEL analysis, bodies that undergo large deformations are meshed with Eulerian elements, while stiffer bodies in the model are meshed with more efficient Lagrangian elements [13].

The aim of this study is to verify that this method could be used in aluminum extrusion tubes using a porthole die. In addition, to observe the result of increasing implementation speed in order to reduce computing time and compare the results obtained by Hyung Ho Jo in 2005 [14].

2 Modeling process

Aluminum extrusion is usually performed at a speed order of millimeters per second; actually, the experiment conducted by Hyung Ho Jo was performed at 1 mm/s and 30 s of duration to view the whole process; however, modeling the process at this speed with CEL technique requires a lot of computing capacity. Therefore, four models were performed at different speeds of the order of m/s to see the effect on the results and computing time required.

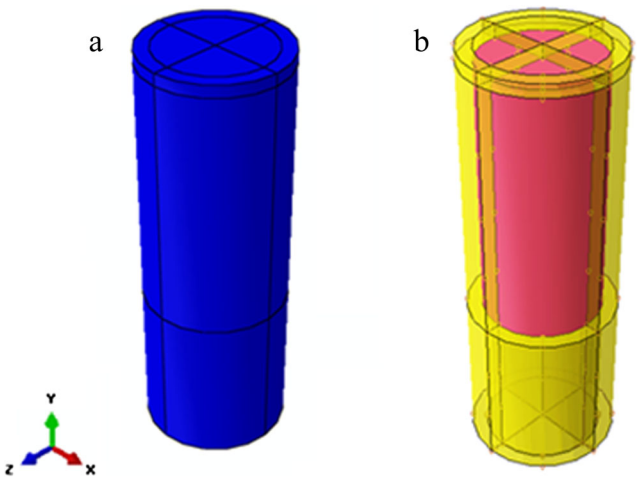

Fig. 2 **a** Eulerian domain and **b** local association material

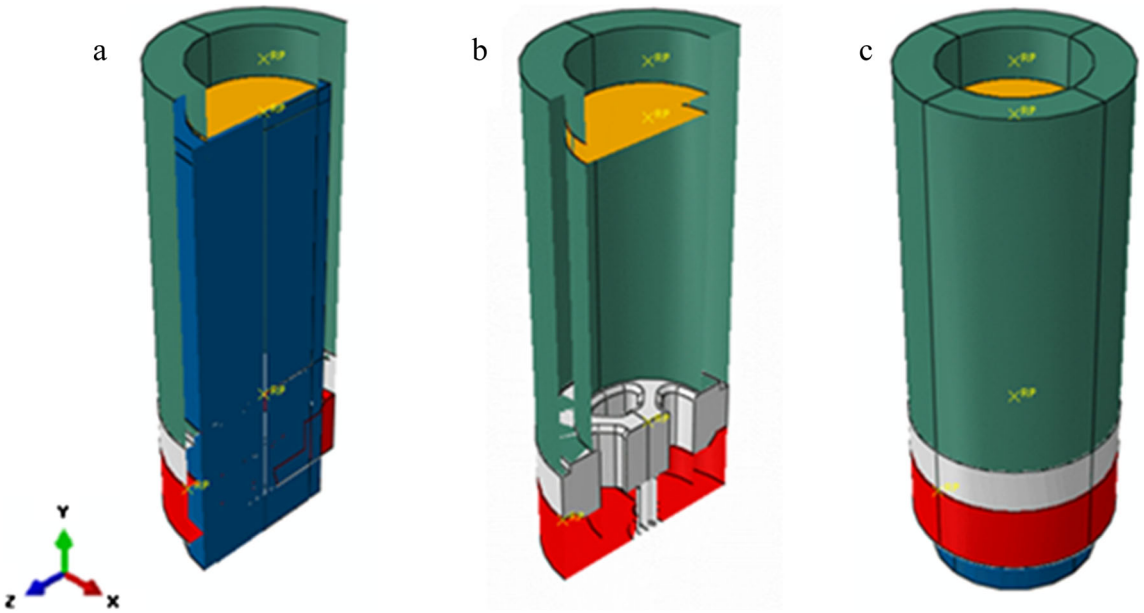

Fig. 3 **a** Cross-section with Eulerian domain, **b** cross-section without Eulerian domain, and **c** 3D model

2.1 Geometry

The workpiece was modeled as a 3D Eulerian solid cylinder without symmetry planes, although partitions were made to improve mesh quality. The Eulerian domain has a 94-mm diameter and is 270 mm long which is shown in Fig. 2**a**; to apply local material associations, partitions at a distance of 100 mm from bottom cover domain were created and another 162 mm from the previous partition, 74.9 mm circular partition was created to define material diameter, so the final billet dimensions are 74.9 mm diameter and 162 mm length.

Die assembly is defined by four components which are upper die, lower die, dummy block, and container; these components are immersed in an Eulerian mesh. Dies were modeled as 3D discrete rigid shell because the deformation of these is not the aim for this work; therefore, it is unnecessary to assign material for these (Fig. 3).

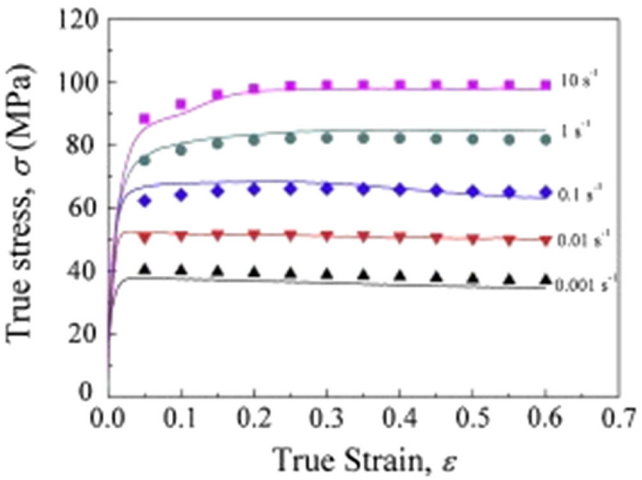

Fig. 4 True stress-strain curve for aluminum 7005–400 °C [16]

2.2 Material properties

The properties of the 7005 aluminum at 400 °C temperature were used. Aluminum density is 2780 kg/m^3, elastic properties were defined according to 72 GPa Young modulus and Poisson's ratio of 0.33 [15]. Figure 4 shows true stress-strain curve for plastic deformation zone at 400 °C temperature, and 1 s^{-1} rate data were used.

2.3 Process parameters

To model the friction phenomenon between dies and material, Coulomb model was established, using general contact option to simulate the interaction between tool surfaces and material.

Table 1 Parameters used for each model

Model	Ram speed (m/s)	Number of steps	Total time model (s)
1	200	3	0.30E-03
2	50	11	1.02E-03
3	20	22	2.11E-03
4	5	16	7.52E-03

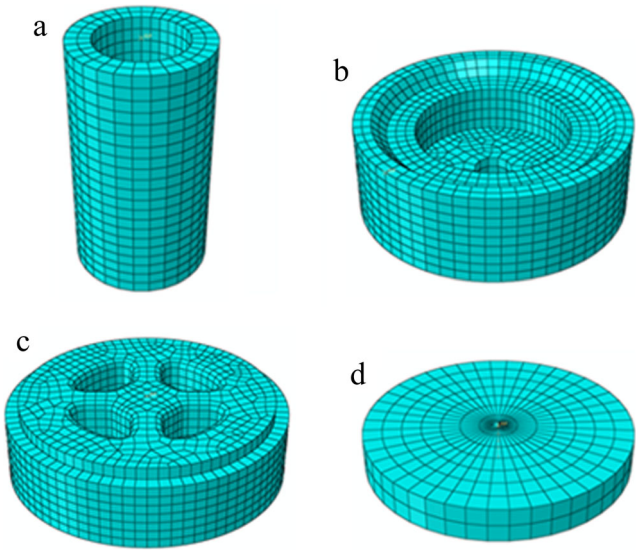

Fig. 5 Discrete rigid tools: **a** container, **b** lower die, **c** upper die, and **d** dummy block

A friction factor between material and tools of 0.7 was defined because it corresponds to extrusion aluminum alloys without lubricant and was used in Hyung Ho Jo experiments in 2005 [14].

The models to develop the sensitivity analysis on ram speed are presented. As a consequence, simulation time was adjusted in order to obtain the same ram displacement, steps are explicit dynamic type, and its characteristics are shown in Table 1.

Upper die, lower, and container are tools that are fixed during the analysis; therefore, an encastre restriction is applied to each reference node, and the part that pushes the material through dies is the dummy block.

2.4 Meshing

Eulerian elements are available for three-dimensional meshing with eight nodes (EC3D8R); Figure 5 corresponds to the tools, where partitions were applied to maintain a good quality mesh. Mesh size influences extruded profile quality; however, due to the Eulerian domain dimensions, it is necessary to be careful because the element size considerably increases computing time.

Considering tube thickness to extrude (1.7 mm), small mesh elements are required; however, to know the elements number to obtain reliable results, various experiments were realized thus it was assigned two elements and 4,091,067 nodes would be required. According to the number of nodes generated, 0.85 mm mesh size element was used such that two elements are present in the opening. Eulerian discretization domain is in Fig. 6.

3 Results analysis

In Fig. 7, final geometry of each experiment is shown; we observe that velocity affects the final tube geometry. Model 1 presents an inhomogeneous flux and therefore a distorted geometry, on the other hand models 2, 3, and 4, present a good geometrical definition of the extruded tube.

3.1 Strain distribution

Figure 8 illustrates strain distribution of model 1 through extrusion process; to visualize the results better, half of 3D model is displayed and will focus on assembly bottom, since this area is where most plastic material deformation takes place. In the initial stage relating to extrusion legs, material flows uniformly and plastic deformation occurs in the contact between material and die, as shown in Fig. 8**a**.

Ram speed is 200 m/s; due to this, vortexes are generated inside the welding zone. In this material, collisions happens in all directions causing an increase of the plastic deformation magnitude. Vortexes generate cavities within the material that can be seen in Figs. 8**b**, **c**, causing defects in extruded product. The geometric space where legs are joined in welding chamber is called welding plane,

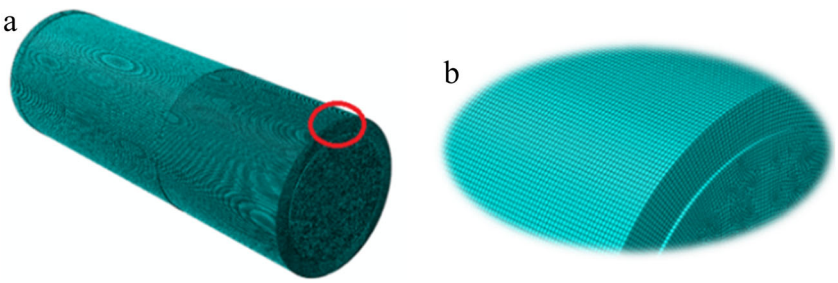

Fig. 6 Mesh used for analysis **a** 3D model and **b** details of mesh application

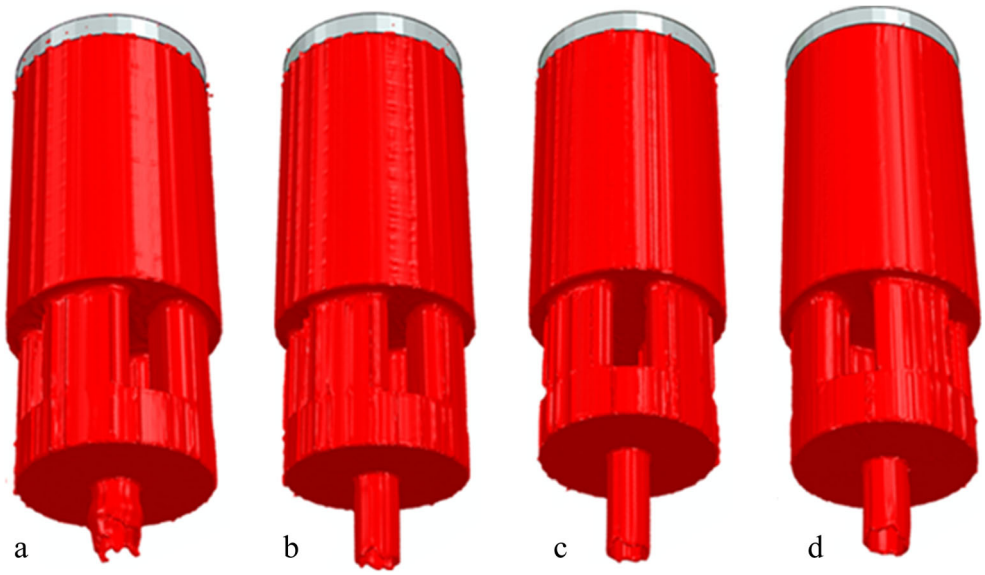

Fig. 7 Final geometry of each model: **a** model 1, **b** model 2, **c** model 3, and **d** model 4

because in those planes material interacts with itself with opposite forces.

Finally, the tube is extruded in Fig. 8**d**; at this stage, greater plastic deformation is the result of the contact between container wall and material, also the greatest strain areas are spread in the welding plane.

Plastic strain distribution behavior in models 2 and 3 is similar to model 4, where the maximum value is in contact between material and die in extrusion legs area.

Plastic strain magnitude existing in model 2 is lower than model 1, since magnitude is reduced by 12 %; however, reduction is 24 % when ram speed is 20 m/s, corresponding to model 3.

Figure 9 shows workpiece deformation evolution for model 4; it is seen that the greatest plastic strain area is concentrated on the interface between material and die where legs are generated, as it is shown in Figs. 9**c**, **d**, while billet central zone has a very small strain illustrated in Fig. 9**a**.

Areas with significant plastic strain are in the welding planes and dead zones, close to those regions shown in Fig. 9**b**; in this area, material interacts with opposite forces and by this action the finished product is expected to be bright and satin.

The difference between minimum and maximum value is not considerable, plastic strain distribution is perceived homogeneous, and central material area has the same deformation value in most internal area; it would allow uniform final mechanical properties of the extruded product, unlike models 2 and 3.

Model 1 presents maximum strain at the welding chamber, while models 2, 3, and 4 show that value in contact between die and material when extrusion legs are generated.

3.2 Stress distribution

Stress distribution in model 1 is shown in Fig. 10. Due to material compression, maximum stress spreads in axial direction through the billet as shown in Fig. 10**a**; friction

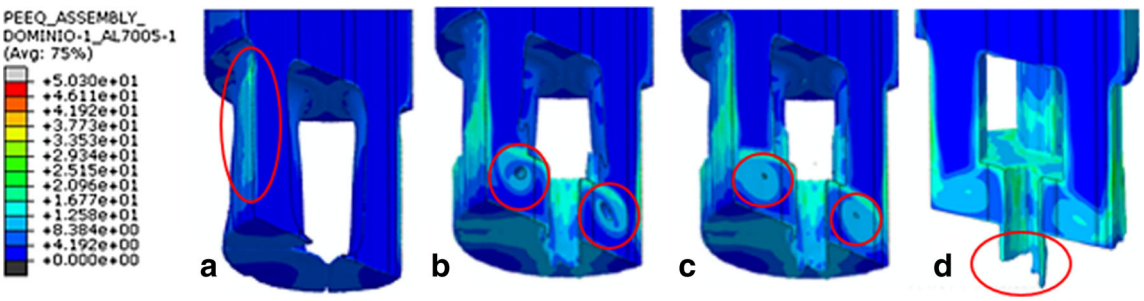

Fig. 8 Plastic strain evolution in model 1

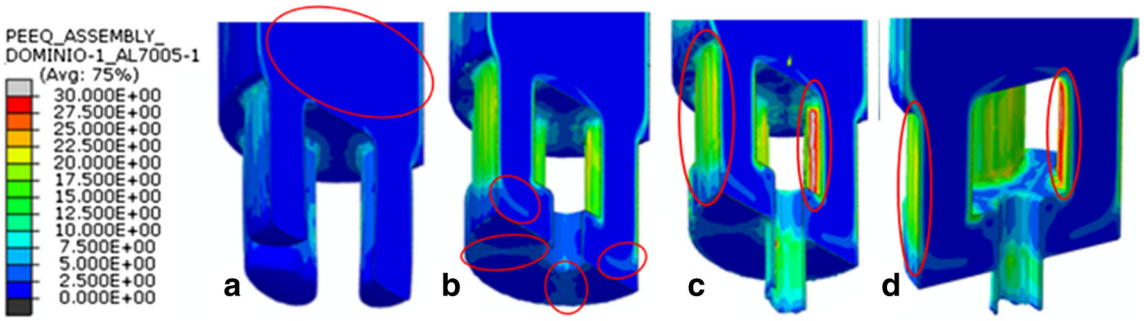

Fig. 9 Plastic strain evolution in model 4

between container walls and material cause maximum stress in this interaction; the value is 80.91 MPa as is shown in Fig. 10**b**.

Figure 10**c** corresponds to material separation and feeding of welding chamber; however, because ram speed is 200 m/s and the cross-sectional area where material flows reduces drastically, material is in maximum stress value for whole process. In central billet area inside the container, there are some regions that present minor values compared to the rest because the central material block descends presenting only compression due to dummy block; this effect is shown in Fig. 10**d–f**

The distribution of the stress progress for model 4 when ram speed is 5 m/s is shown in Fig. 11. In compression material stage inside the container, the stress in models 2, 3, and 4 is homogeneously distributed because it is increasing gradually, not suddenly as in model 1.

Due to the container geometry and the friction on the walls, stresses are distributed in a cone shape which promotes chevron craks; this feature is shown in Fig. 11**a**, **b**. Stress level is reduced when material flows freely into the legs as in Fig. 11**c** and increases when it presents contact with the lower die (Fig. 11**d**).

When tube extrusion begins, there is a central region that presents minor stress values in comparison with the remaining material, as illustrated in Fig. 11**e**.

As in previous models, maximum values are shown in contact with container walls; in feeding and welding planes, maximum value is 79 MPa, which is the same as in models 2 and 3; however, the covered area for this value is lower than other models.

3.3 Material flow

The flow vector visualization when ram speed is 200 m/s is shown in Fig. 12. In Fig. 12**a**, the billet division occurs in four legs that later feed the welding chamber; when this happens, material is accelerated because the cross-sectional area is minor and can flow freely until it collides with the lower die, as shown in Fig. 12**b**.

In Fig. 13**a** is observed that extrusion legs are joined at the bottom of the welding chamber and start filling this through the welding planes generation; when material collides with the top of the camera (Fig. 13**b**), cavities are generated. Extrusion legs are thin and do not cover the whole porthole area, so the first chamber is filled and then the material moves through free spaces inside portholes,

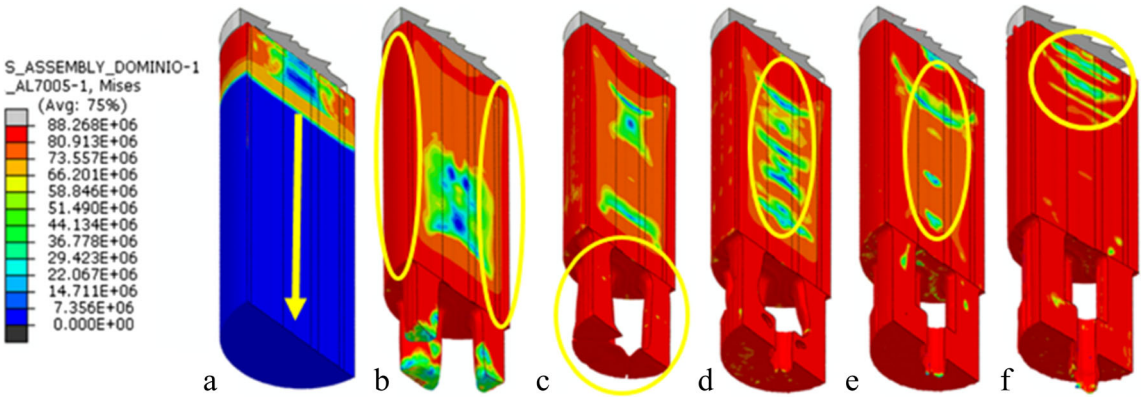

Fig. 10 Stress evolution in model 1

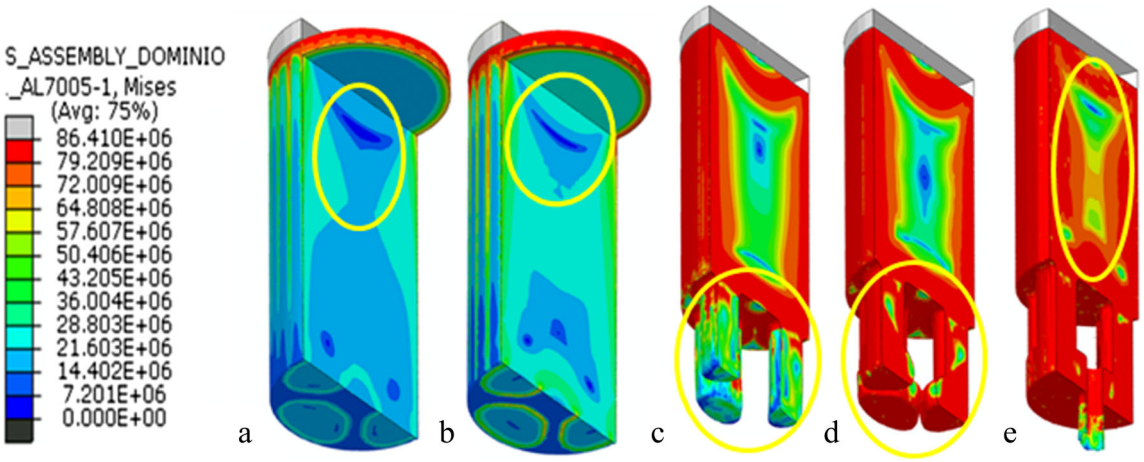

Fig. 11 Stress evolution in model 4

causing the material flow backwards ram sliding, as shown in Fig. 13**c**.

When portholes are completely filled, the opposite speed profiles collapse with each other and present a region as seen in Fig. 14**a**, where three different areas are distinguished. In the first, vortexes are generated during filling chamber due to large rate changes in that area; the second region is blocked up, and the third region is the one that induces the new velocity profile due to ram displacement.

Figure 14**b** corresponds to tube extrusion. This shows the presence of vortexes that continues; the opening forming tube geometry forces the material to flow in laminar form; however, velocity profile indicates that distribution is not homogeneous and therefore tube has defects and does not present a suitable geometry

Since application speed is lower in models 2 and 3, legs are extruded uniformly and expand to the contact with the base die, hence to contact between them in welding planes, the lower die is nearly filled, unlike model 1.

Dead zones allow the flow of material toward the opening in laminar form as shown in Fig. 15**c**. Figure 15**b** shows in detail their presence and how they affect material flow. Across the corner in the lower die, the presence of dead zones is concentrated and a 3D parabola region is produced; it is necessary to clarify that lines that enhance visualization of dead zones were drawn.

In model 4, material speed in the cavity that dies generate is uniform like in ideal extrusion process behavior; therefore, product corresponds to required dimensions. Due to friction in the bearing die, material flows through the outlet cavity as laminar.

Figure 16 shows welding chamber filling. When extrusion legs reached lower die base, they begin to increase their base area as shown in Figs. 16**a**, **b**. Due to the rate, when such entities merge, the chamber is practically full,

Fig. 12 Material flow in model 1

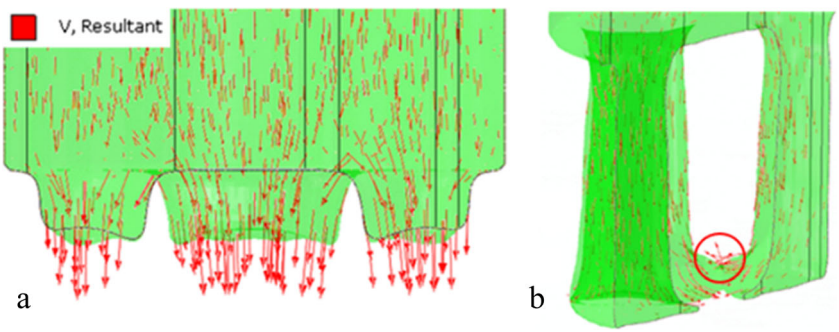

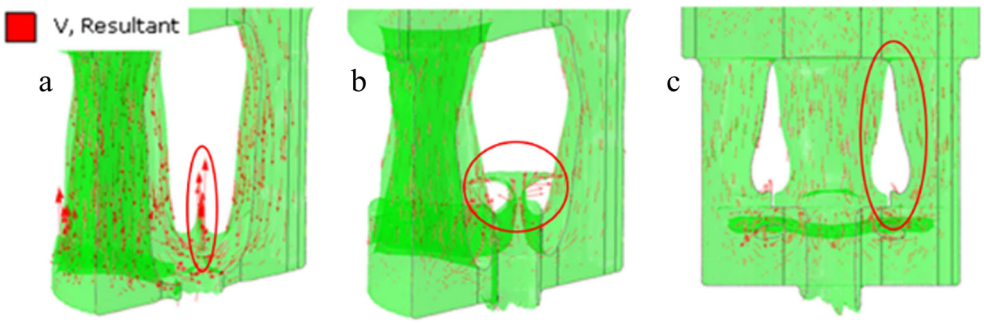

Fig. 13 Material flow in model 1

unlike previous models where extrusion legs bonded first and then through welding planes, the welding chamber was filled as in model 1 or had higher empty areas as models 2 and 3

In porthole dies designs, dead zones are considered in such way that metal which generates welding planes is "virgin" in other words is contaminants free such as oxides that are present during thermal treatment before extrusion [17].

Dead zones are generated on the welding chamber base as shown in Fig. 17**b**. Material dead zones do not mean that there is no speed; actually, those areas where large speed differences occur in nearest regions, for aluminum a dead zone is defined as the region in which material speed is from 0 to 10 % of application rate [18].

In models 2, 3, and 4, tube extrusion was carried out uniformly; dead zones help the material to flow at the same speed in the whole periphery.

3.4 Extrusion load

Blue curve in Fig. 18 corresponds to load displacement for model 1. At the first stage, there is an increase in extrusion force because billet diameter is smaller than the container diameter; the difference is 0.1 mm. Force

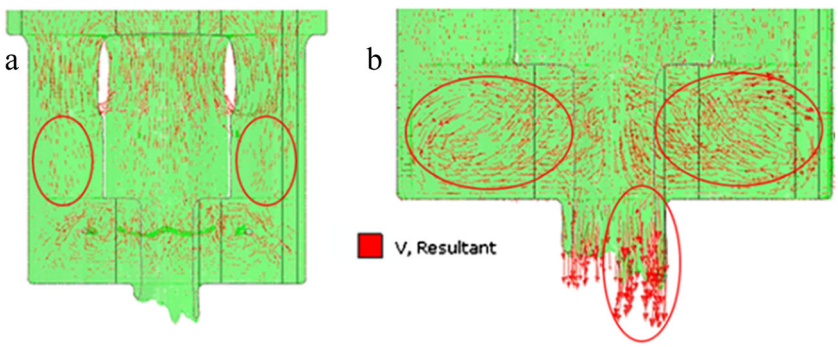

Fig. 14 Tube extrusion in model 1

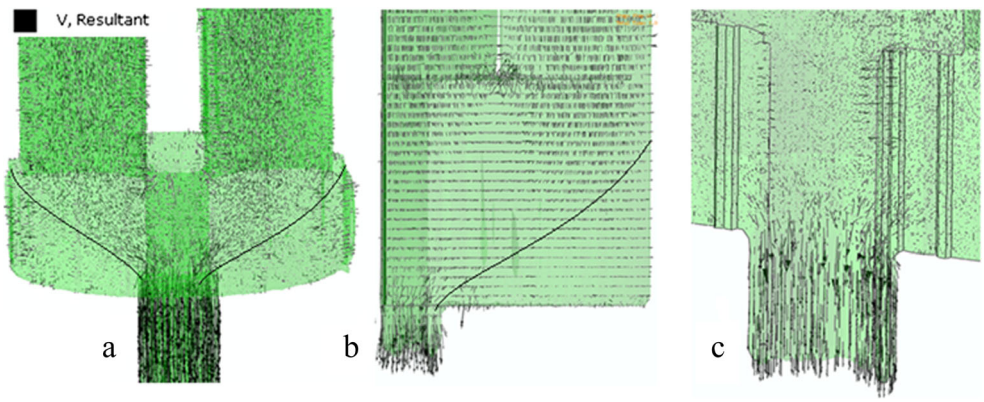

Fig. 15 Dead zones presence in model 3

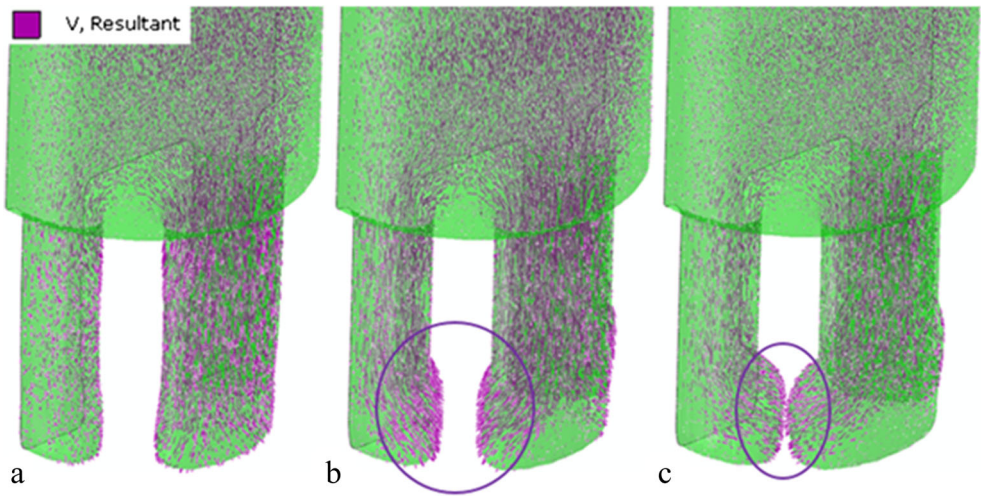

Fig. 16 Welding chamber filling in model 4

magnitude reaches 1360 t because of material compression and reduces this value to 437 t when legs are extruded.

When dummy block moves 33 mm, the welding chamber was completely filled and load magnitude increases to 802 t; at 40 mm, extrusion tube starts and it begins to increase required extrusion force because material initial contact area increases too.

On the other hand, the red curve in Fig. 18 is the load-displacement curve for model 2; it is observed that the force increases to 530 t and decreases its value when material is

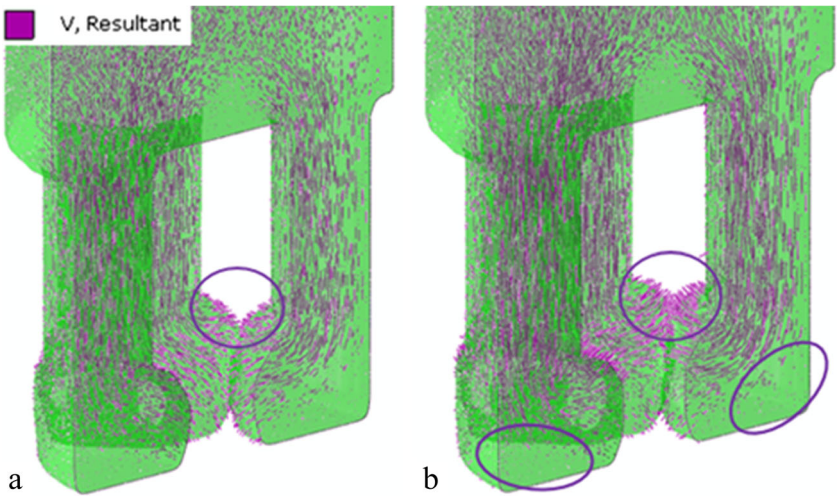

Fig. 17 Dead zones presence in model 4

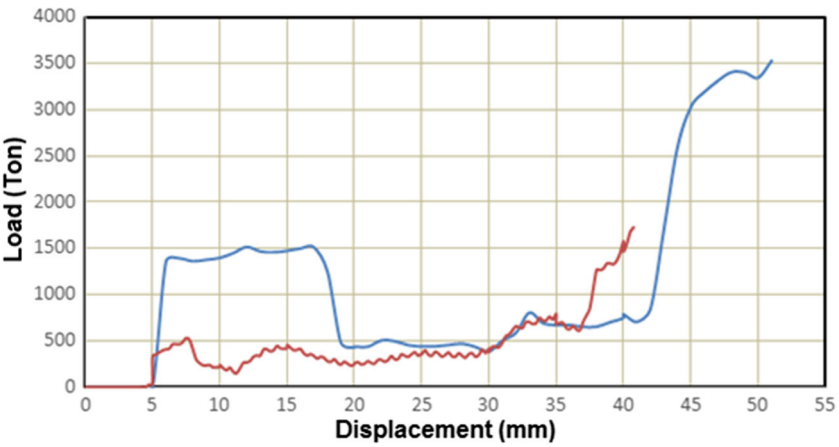

Fig. 18 Load-displacement curves for models 1 and 2

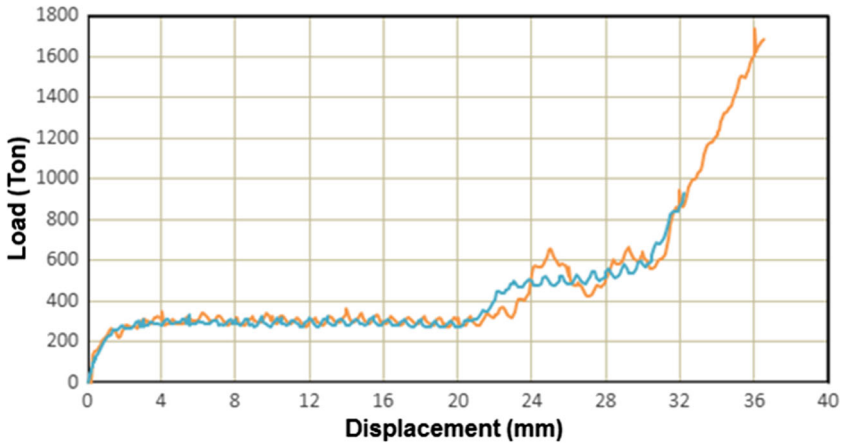

Fig. 19 Load-displacement for models 3 and 4

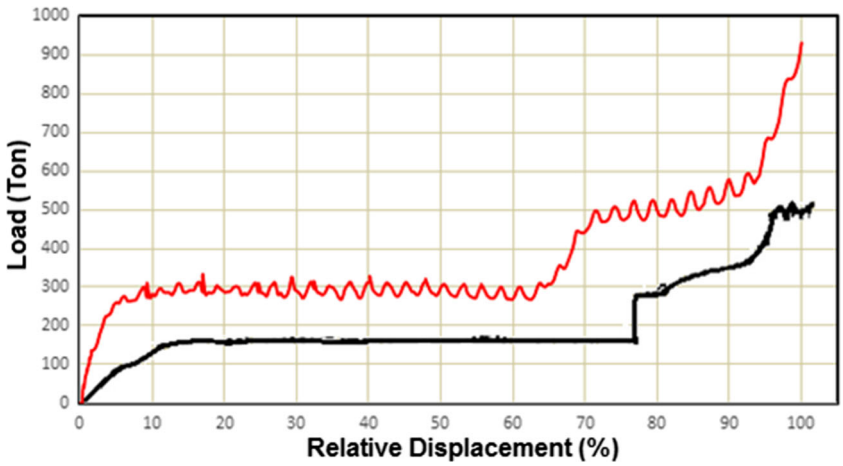

Fig. 20 Load-displacement for model 4 and experimental

divided into legs. There are variations of around 349 t, and the increase comes to 32 mm displacement; in this stage, the welding chamber is completely filled and tube extrusion begins.

The load-displacement curve for model 3 is shown in Fig. 19 in orange; load reaches 220 t value and it continues until dummy block displaces 24 mm. From 25 to 30 mm, the welding chamber is filled; at this stage, two peaks are seen, the first occurs when legs touch the bottom die and material moves laterally; the second is generated when legs come together and fill the empty areas inside welding chamber. When ram is at 32 mm displacement, the tube extrusion starts; due to opposite forces in opposite directions, there is an increase in required load extrusion.

The graph obtained for model 4 is shown in Fig. 19 represented in blue, where it is seen that force reaches 273 t value and ranges in that value until there is 20 mm of ram displacement. Magnitude increases in 21 mm because extrusion legs make contact with the bottom die base and begins filling chamber, reaching a 539 t value; tube extrusion begins when dummy block is at 29 mm. For that reason, the force needed increases.

Figure 20 shows the comparison between model 4 and the experimental graph obtained by Hyung Ho Jo, where it can be seen that behavior is similar. Dummy block displacement is

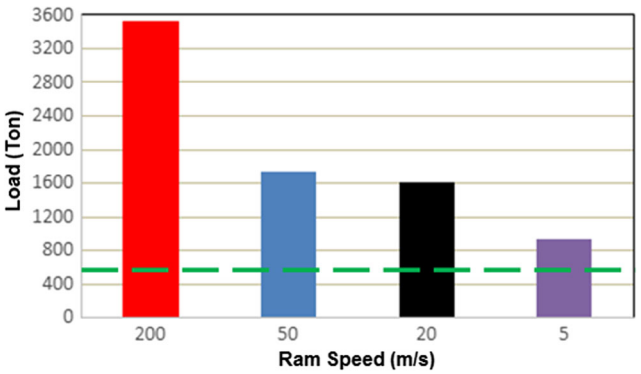

Fig. 21 Comparison of maximum force values for each model

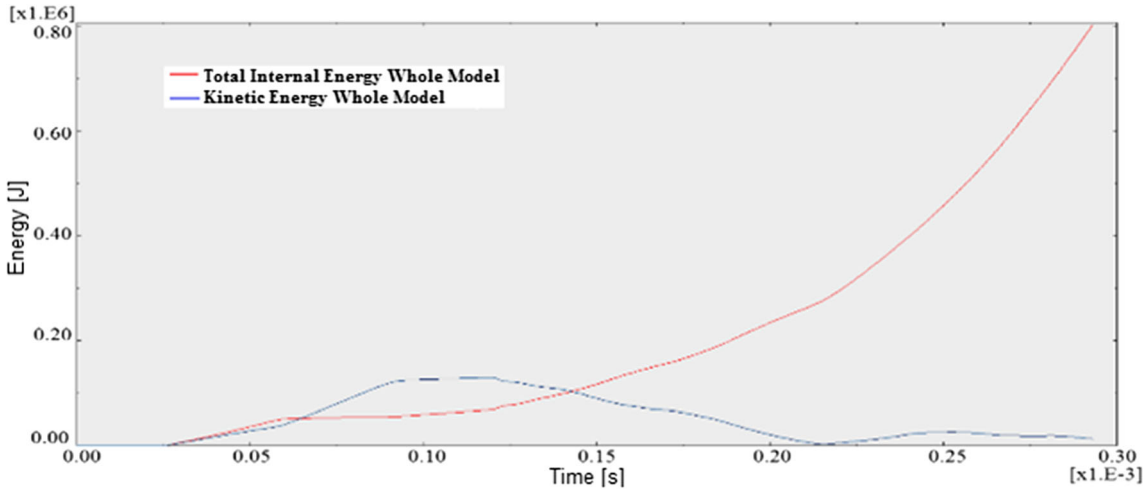

Fig. 22 Kinetic and total energy graph for model 1

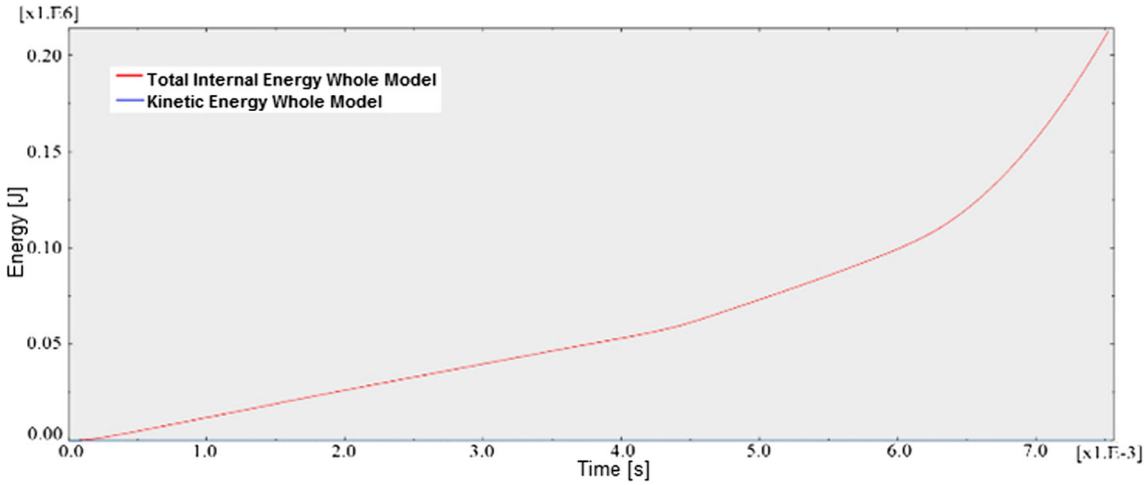

Fig. 23 Kinetic and total energy graph for model 4

different in both experiments and ram rate is too; however, extruded product length is similar

Table 2 Stress values in MPa at tube extrusion

Stage	Ram speed (m/s)			
	200	50	20	5
Billet central region	7.35	7.21	7.19	7.20
Welding planes	80.91	79.36	79.10	79.20
Material contact with dies at extrusion legs	80.91	79.36	79.10	79.20
Interface with dead zones	80.91	79.36	79.10	79.20
Tube extrusion	80.91	72.15	71.90	72.00

The maximum value is 3525 t when ram speed is 200 m/s, 1725 t when the speed is 50 m/s, 1683 t when the speed is 20 m/s, and 931 t when dummy block moves to 5 m/s. The maximum value inside the executed experiments was 530 t; the comparison of these values is shown in Fig. 21.

A model is considered valid if kinetic energy does not exceed 5 to 10 % of total internal energy [19]. Figures 22 and 23 correspond to the comparison of these energies for each event.

In Fig. 22, kinetic energy exceeds internal energy value; therefore, model 1 is invalid. Even the geometry of the tube is not the best because there are defects.

On the other hand, the energy graphics for models 2, 3, and 4 are right; however, this condition does not ensure that model is completely valid. Strains present in each model are different, diminishing the magnitude in function of speed; on the other hand, stress distribution is similar in all simulations,

Table 3 Force extrusion values obtained in different stages of the process, the units are tons

Stage	Ram speed (m/s)				Experimental model
	200	50	20	5	
Billet compression	1360	329	220	222	150
Extrusion legs begins	1458	530	287	273	150
Extrusion legs contact with welding chamber base	437	349	617	449	260
Full welding chamber	802	611	861	534	330
Tube extrusion	3525	1725	1683	931	530

therefore these results are reliable and they can help to make decisions.

4 Discussion

The material strain distribution depends on the implementation speed, because values are high if speed is, however, pass over magnitudes; it can be seen that in models 2, 3, and 4, strains behavior is similar. Maximum value is present in the contact between material and die; an intermediate strain zone was found in welding planes and minimal strain in the central billet area.

Stresses are similar for all models and there are differences of 1 to 2 % between them taking as a reference model 4 that generates a better distribution and geometry; this indicates that the stress evolution in whole process is reliable. To choose correctly the extrusion equipment, extrusion force is required; this parameter is dependent on ram speed.

Table 2 lists the data stress obtained of the four models; it is clear that the values presented correspond to the extrusion of the tube and not earlier stages such as compression or division of material.

For flow analysis, vector visualization was possible and let us see that those models exhibit the same behavior in the welding zones formation, the filling welding chamber, and tube extrusion; therefore, those results are valid unlike model 1.

According to the vector visualization, the importance of dead zones presence was observed; their appearance elevate the required force magnitude, which impacts on a higher capacity press; however, material tends to generate its own attack angles.

Collecting the results obtained in the extrusion force required in different stages is shown in Table 3. This is seen that with decreasing speed of dummy block decreases the magnitude of the extrusion force, the maximum value in all models presented in tube extrusion because the material has contact with four different areas, the container wall, upper and lower wall, and bearing.

Energy curves for model 1 did not present the desired behavior, since high speed affects inertial variables in the model, causing a bad distribution and irregular extruded product geometry; nevertheless, models 2, 3, and 4 showed the desired behavior. However, according to the results of the analyzed variables, it is concluded that the stress and the material flow behavior are the only ones valid.

5 Conclusions

The coupled Eulerian-Lagrangian method (CEL) has been adopted to model the porthole die extrusion at different ram speed in order to obtain a 1.7 mm aluminum tube; the results were compared to the experimental results obtained by Hyung et al. in 2005. Using CEL analysis was possible without using re-meshing criteria, distortion mesh control, or separation and welding criteria that other methods require.

Extrusion force decreases according to ram speed reduction as we expected, so these results should be taken with caution; however, the downward magnitude trend, makes sure that if you have suitable computing capacity and the process is simulated into a nearest real speed, the result would approximate the experimental values. On the other hand, material flow behavior is valid if kinetic energy does not exceed 5 to 10 % of total internal energy models.

Extrusion is not an isothermal process, and thermomechanical models will improve material flow description; in addition, two additional variables would be obtained: the temperature profile and the heat flux.

References

1. Liu G, Zhou J, Duszczyk J (2007) FE Analysis of metal flow and weld seam formation in a porthole die during the extrusion of a magnesium alloy into a square tube and the effect of ram speed on weld strength. Journal of Materials Processing Technology, Netherlands
2. Padmanathan K (2013) Parameter optimization of the process of AA6XXX and AA7XXX series aluminium extrusion. Auckland University of Technology, New Zealand
3. Christopher P, Yannis P (2014) Strength and ductility evaluation of cold-welded seams in aluminum tubes extruded through porthole dies. Materials and design, USA

4. Xianghong W, Guoqun Z, Yiguo L (2006) Numerical simulation and die structure optimization of an aluminum rectangular hollow pipe extrusion process. Materials Science & Engineering, China
5. Kloppenborg T, Schwane M, Khalifa N, Tekkaya AE, Brosius A (2012) Experimental and Numerical analysis of material flow in porthole die extrusion. Key Engineering Materials, Germany
6. Li L, Zhang H, Zhou J, Duszczyk J, Li GY, Zhong H (2008) Numerical and experimental study on the extrusion through a porthole die to produce a hollow Mg profile with longitudinal weld seams. Materials and Design, Netherlands
7. Ceretti E, Fratini L, Gagliardi F, Giardini C (2009) A new approach to study material bonding in extrusion porthole dies. Annals of the CIRP, Italy
8. Bariani P, Bruschi S, Ghiotti A (2006) Physical simulation of longitudinal welding in porthole die extrusion. Annals of the CIRP, Italy
9. Gagliardi F, Ambrogio G, Filice L (2012) On the die design in AA6082 porthole extrusion. Manufacturing Technology, Italy
10. Junquan Y, Guoqun Z, Liang C (2016) Analysis of longitudinal weld seam defects and investigation of solid-state bonding criteria in porthole die extrusion process of aluminum alloy profiles. Journal of Materials Processing Technology, China
11. Zhang Z, Hou W, Huang D, Xie J (2012) Mesh Reconstruction Technology of welding process in 3D FEM simulation of porthole extrusion and its application. Procedia engineering, China
12. Simulia Dassault Systemes (2010) Coupled Eulerian Lagrangian Modelling Tecniques. Lecture 4
13. Simulia Dassault Systemes (2016) Overview of Eulerian analyses. Abaqus User's Guide Lecture 28.1
14. Jo H, Lee S, Jung S (2005) A non-steady FE analysis of Al tubes hot extrusion by a porthole die. Journal of Materials Processing Technology, South Korea
15. Matweb (2015) Aluminium 7005 Data Sheets. Material Property Data, USA
16. Chen L, Guoqun Z (2014) Constitutive analysis of homogenized 7005 aluminium alloy at evaluated temperature for extrusion process. Materials and Design, China
17. Zhong Z, Saka H, Kim T (2005) A bonding map for Cu and Al plates by pressure welding at cold and warm temperatures. Materials Science Forum, Sweden
18. Koopman Albertus J (2008) Analysis tools for the design of aluminium extrusion dies, PhD Thesis, Twente University, Netherlands
19. Xingui H, Lin H (2008) 3D FE Modelling simulation of cold rotatory forging of a cylinder workpiece. Material and Design, China